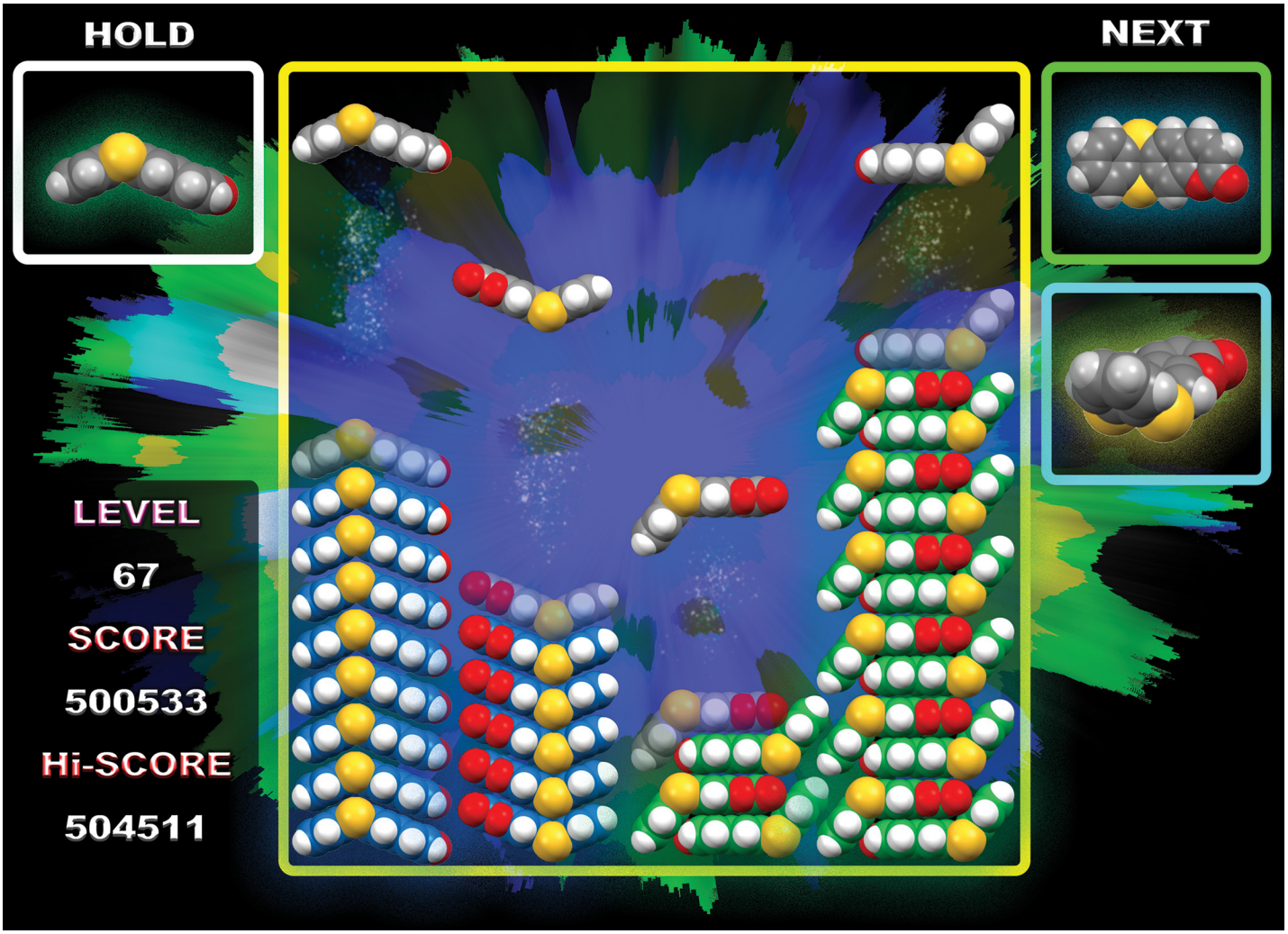

Showcasing research from the Department of Chemistry, School of Science at Kitasato University, Kanagawa, Japan.

A folded mechanochromic organic fluorophore based on thianthrene-fused coumarin

The folded luminophore (6,7-BDTC), a fusion of thianthrene and coumarin, was found to exhibit light blue and green crystallization-induced emission depending on the stacking pattern. In powder, the emission color can be changed even by mechanical stimulation.

Image reproduced by permission of Masafumi Ueda from *Chem. Commun.*, 2026, **62**, 2208.

As featured in:

See Masafumi Ueda *et al.*, *Chem. Commun.*, 2026, **62**, 2208.

ROYAL SOCIETY OF CHEMISTRY

rsc.li/chemcomm

Registered charity number: 207890

ChemComm

COMMUNICATION

View Article Online
View Journal | View Issue

Cite this: *Chem. Commun.*, 2026, **62**, 2208

Received 15th September 2025,
Accepted 10th December 2025

DOI: 10.1039/d5cc05320j

rsc.li/chemcomm

A folded mechanochromic organic fluorophore based on thianthrene-fused coumarin

Masafumi Ueda, *[a] Asuka Uehara,[a] Kazuteru Usui [b] and Masashi Hasegawa [a]

The powder samples of a novel thianthrene-fused coumarin dye (6,7-BDTC) demonstrated pronounced mechanochromic luminescence, shifting from light-blue to green emission upon mechanical stimulation. X-ray crystallography of polymorphs with different emission colors revealed that this responsiveness originates from variations in the packing mode induced by the D–A type folded structure. These results demonstrate that introducing a folded π-conjugated framework into the coumarin core enables control over the packing mode and emission properties in the solid state.

Coumarin (2*H*-chromen-2-one) is a bioorganic aromatic lactone that has garnered considerable attention in pharmacology and physiology.[1] Its versatile structure allows facile chemical modification, leading to the development of highly efficient luminescent dyes, such as donor–acceptor-type coumarin derivatives, which have a strong presence as key components in organic optical devices.[2] To tune the photophysical properties and improve stability, numerous π-expanded coumarins with unique molecular skeletons have been developed. Most of these derivatives exhibit photophysical properties stemming from their rigid and planar π-conjugated structures.[3] Conversely, helical π-expansion of the coumarin dyes imparts chiroptical activity,[4] while curved or polycyclic π-systems incorporating coumarin often produce bright orange to red emissions in both solution and the solid state.[5] Thus, the molecular geometry of π-expanded coumarins critically determines their photophysical properties, and the construction of novel π-frameworks remains essential for expanding the design diversity of coumarin-based luminophores.

Among the possible π-extension strategies, double sulfur bridging (exemplified by the thianthrene skeleton) is a powerful method to enhance conjugation through sulfur orbitals. However, the C–S–C bond introduces structural bending due to the lone pairs on sulfur, resulting in folded π-conjugated architectures. Such a folding often leads to dynamic conformational changes between the ground (S_0) and the lowest excited (S_1) states, where nonradiative decay dominates and emission efficiency decreases. Indeed, thianthrene itself exhibits low fluorescence efficiency (Φ_F = 2%) in THF solution but shows room-temperature phosphorescence in the crystalline state with enhanced efficiency (Φ_P = 25%) owing to restricted molecular motion.[6] These findings highlight that molecular immobilization in the solid state can suppress non-radiative decay, a key in AIEgens[7] and in the design of stimuli-responsive luminescent materials.[8] In addition, the π-systems possessing stereospecific frameworks impose steric effects on molecular packing and can modulate π–π interactions, thereby influencing luminescence efficiency and solid-state color tuning.[9] Control of such intermolecular arrangements—self-aggregation, hydrogen bonding, encapsulated solvents, or mechanical stress—offers a route to mechanoresponsive materials.[10] However, it remains difficult to clearly understand the excited states of the aggregate, and there is little evidence to resolve the question of how applicable π-expanded coumarin dyes incorporating a folding skeleton are to these phenomena.

To address this, we newly designed a novel coumarin dye, 6,7-BDTC, by fusing a folded thianthrene core with a planar coumarin framework (Fig. 1). This structure combines π-extension with a defined folding geometry (dihedral angle:

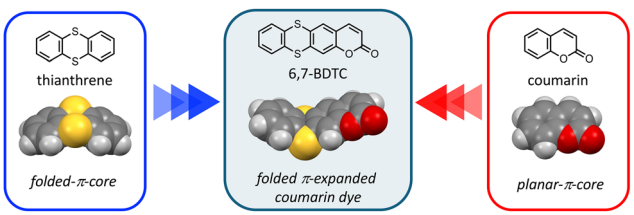

Fig. 1 Chemical and optimized structures of 6,7-BDTC, thianthrene, and coumarin. Optimizations were estimated by the CAMB3LYP/6-31G(d,p) level.

[a] *Department of Chemistry, Graduate School of Science, Kitasato University, 1-15-1 Kitazato, Minami-ku, Sagamihara, Kanagawa, 252-0373, Japan. E-mail: msfmueda@kitasato-u.ac.jp*

[b] *Faculty of Pharmaceutical Sciences, Showa Pharmaceutical University, 3-3165 Higashi-tamagawagakuen, Machida, Tokyo, 194-8543, Japan*

129°), enabling the study of how molecular shape governs luminescence behavior in both dilute solutions and solid assemblies. Also, enhanced emission efficiency based on the intramolecular donor–acceptor structure of the coumarin core can be expected through electron donation from the thianthrene core.[11,12] This asymmetric folding structure, in contrast to conventional planar coumarin dyes, has the potential to induce changes in the stacking pattern within molecular assemblies and control the overlap of conjugated π-planes. This paper describes the synthesis of 6,7-BDTC and its emission behavior in both single-molecule dispersions and solid states.

The synthetic route to 6,7-BDTC is shown in Scheme 1. 3,4-Difluoroanisole (**1**) was treated with $TiCl_4$ and dichloromethyl methyl ether (Rieche formylation) to afford 4,5-difluoro-2-methoxybenzaldehyde (**2**). Compound **3** was prepared from the Wittig reaction of **2** with ethyl(triphenylphosphoranylidene)acetate. 6,7-Difluorocoumarin (**4**) was formed by intramolecular annulation of **3** in the presence of Lewis acid. Ultimately, the target compound 6,7-BDTC was obtained *via* aromatic nucleophilic substitution of 1,2-benzenedithiol with **4** in a good yield. Two crystalline polymorphs (crystals **I** and **II**) obtained by slow evaporation of acetone and EtOAc revealed that 6,7-BDTC folds at the dihedral angles of 132 and 126° along the S···S axis (Fig. S30).

The absorption and emission spectra of 6,7-BDTC in various solvents were recorded to uncover the photophysical properties (Fig. 2a and Table 1). Three main absorption bands at 350, 285, and 255 nm were observed for various solutions of 6,7-BDTC (c = 0.01 mM). The longest wavelength absorption band at 350 nm was attributed to the transition (oscillator strength (f) = 0.2027) from HOMO to LUMO estimated by quantum chemical calculations (Fig. S35 and Table S3). The second and third absorption bands were attributed to mixed configurations with $S_0 \rightarrow S_{3,4}$ (f = 0.1979 and 0.1871) and $S_0 \rightarrow S_{11}$ (f = 0.2007) as the main transitions. Focusing on the frontier molecular orbitals, the HOMO of 6,7-BDTC was distributed throughout the entire molecule, while the LUMO was mainly localized on the coumarin core (Fig. 2b). This suggests that 6,7-BDTC adopts a donor–acceptor-type intramolecular charge-separated structure from the thianthrene to the coumarin core during the transition process.[12]

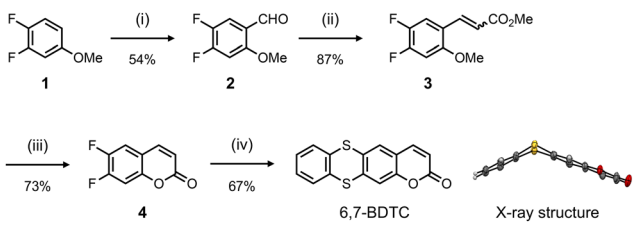

Scheme 1 Synthetic route for 6,7-BDTC: (i) $TiCl_4$, dichloromethyl methyl ether, CH_2Cl_2, 0 °C → ambient temperature; (ii) ethyl(triphenylphosphoranylidene)acetate, CH_2Cl_2, 40 °C, (E/Z = 4 : 1); (iii) BBr_3, CH_2Cl_2, 0 → 50 °C; (iv) 1,2-benzenedithiol, Cs_2CO_3, DMF, 120 °C, and X-ray structure of 6,7-BDTC (crystal **I**). The ellipsoids indicate a 50% probability of formation.

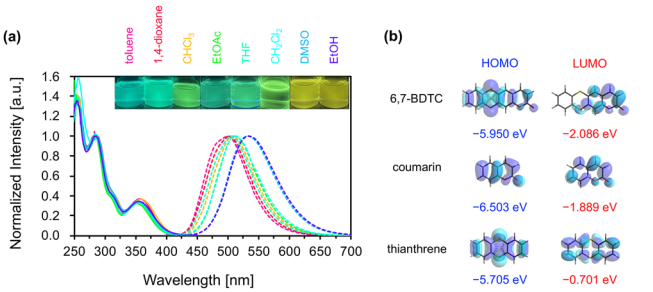

Fig. 2 (a) Normalized absorption (solid line) and emission (dashed line) spectra of 6,7-BDTC in various tested solvents, and their photographic images were recorded under the irradiation of a UV lamp (365 nm). (b) Frontier molecular orbitals of 6,7-BDTC, coumarin, and thianthrene.

Table 1 Photophysical properties of 6,7-BDTC in the tested solvents. K_r = Φ_F/τ, K_{nr} = $1/\tau - K_r$

Solvent	λ_{abs} [nm]	λ_{em} [nm]	Φ_F [%]	τ [ns]	K_r [ns^{-1}]	K_{nr} [ns^{-1}]
Toluene	356	500	32	5.70	0.056	0.177
1,4-Dioxane	355	502	34	6.97	0.048	0.144
$CHCl_3$	359	511	38	7.14	0.053	0.141
EtOAc	353	506	32	6.48	0.049	0.156
THF	354	508	30	7.07	0.042	0.142
CH_2Cl_2	353	516	47	8.08	0.058	0.125
DMSO	355	531	40	9.12	0.043	0.110
EtOH	356	533	29	7.00	0.041	0.144

The solutions of 6,7-BDTC exhibited a slight solvatochromic effect in the emission spectra with a redshift of *ca.* 0.15 eV from green to yellow. The Lippert–Mataga plots showed a positive correlation between the Stokes shift (1.0 to 1.2 eV) and solvent parameters ($E_T(30)$)[13] (Fig. S20); the polarity and hydrogen bonding effect appeared to influence the emission wavelength (Fig. S21). The structural optimization at the CAMB3LYP/6-31G(d,p) level for the S_0 and S_1 states suggested a dynamic conformational change from the folded to flattened state, with the dipole moment increasing slightly from 3.997 to 4.017 D (Fig. S36). These results indicate that the contribution of the resonance effect based on intramolecular charge-transfer in the flat S_1 state lowered the energy level in highly polar solvents (Fig. S37).[12] Additionally, it was found that 6,7-BDTC exhibits concentration quenching (Fig. S22). Fluorescence quantum yields (Φ_F) were 29–47% regardless of the solvent polarity or viscosity. These were lower than that of 4-methyl-7-methylthiocoumarin (81%)[14] but higher than that of planar coumarinacene (24%).[15] Conversely, relatively long lifetimes (τ) of 5.7 to 9.1 ns with a single-exponential fluorescence decay were observed (Fig. S24 and Table S1). In all solutions, the nonradiative rate constant (K_{nr}) was higher than the radiative rate constant (K_r), suggesting that the thermal deactivation process induced by dynamic conformational changes dominates during the decay process from flat S_1 to folded S_0.

The powder sample of 6,7-BDTC exhibited light blue fluorescence, and when this powder was ground in a mortar, the luminescence color changed to green (Fig. 3 and SI, Movie file). The difference between the two states was observed as a slight

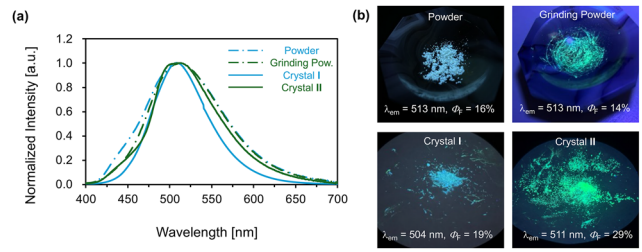

Fig. 3 (a) Emission spectra of 6,7-BDTC in the solid state: powder (light blue dashed line); grinding powder (green dashed line); crystal **I** (light blue solid line); and crystal **II** (green solid line). (b) Photographic images of 6,7-BDTC in the solid state were recorded under irradiation by a 365 nm UV lamp.

change involving a slight redshift and spectral broadening. This suggests that 6,7-BDTC can serve as a promising mechanochromic fluorophore. After vapor exposure to CH_2Cl_2, the greenish emission color returned to its original light blue (Fig. S28). This process was reversible over multiple cycles. The Φ_F values (normal powder: 16%; grinding powder: 14%) were slightly lower than those in solution. Despite exhibiting concentration quenching, the emission might occur because the folded 6,7-BDTC was tightly immobilized within the assemblies, suppressing the conformational changes from S_1 to S_0. Fluorescence lifetime measurements revealed that both normal and ground powder samples exhibit a double-exponential decay process. For the normal powder, the decay curve showed that the short-lived τ_1 (1.45 ns) component accounted for 74%, while the long-lived τ_2 component accounted for 26% (5.49 ns, average: 2.51 ns). For the ground powder, τ_1 (2.67 ns) accounted for 26% and τ_2 (6.86 ns) accounted for 74% (average: 5.75 ns, Fig. S25 and Table S1). The excitation spectra of both powders showed slight changes in relative intensity (Fig. S26). These results suggest the presence of two types of luminescent species in each powder based on the stacking order of the aggregates. The ratio of short τ_1 to long τ_2 is reversed before and after grinding, indicating that mechanical stimulation relatively increased the long-lived luminescent species (Fig. S29). Since its lifetimes resemble those in solution, this suggests that the electronic properties of the excited state in the grinding powder locally approach those of a single-molecule state.

Fortunately, the obtained crystal polymorphs **I** and **II** exhibited light blue and green emissions, respectively (Fig. 3b, bottom). Therefore, we compared them using X-ray crystallography to gain further insights into the intermolecular packing order (Fig. 4). The light blue emissive crystal **I** had a space group of *I*2/*a*, and 6,7-BDTC aligned along the *b*-axis, maintaining the folded skeleton (the dihedral angle: 132°). The intermolecular stacking distance along the *b* axis was 3.860 Å. On the long side of 6,7-BDTC, a hydrogen bonding network was formed with neighboring molecules by C–H···O and C–H···S interactions (Fig. S31). On the short side, at the lactone moiety, 6,7-BDTC formed strong interactions, hydrogen bonds between the oxygen atom of the carbonyl group and the hydrogen atom at the 3-position of the coumarin. Conversely, green emissive

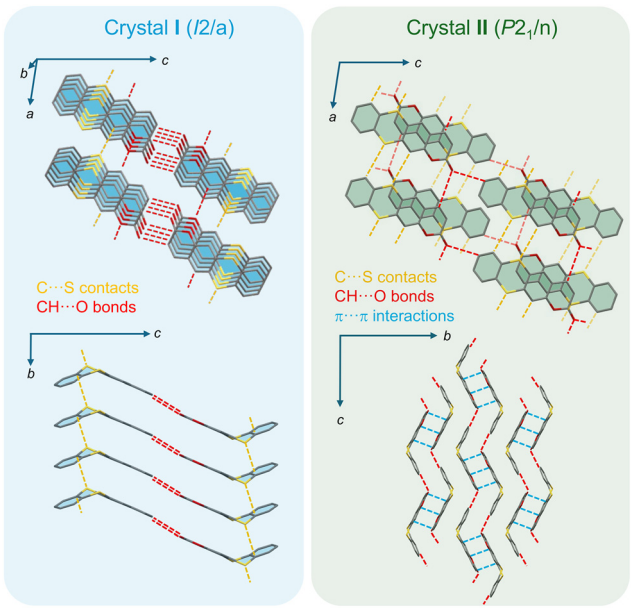

Fig. 4 Crystal structures of crystals **I** and **II** of 6,7-BDTC. Hydrogen atoms are not shown for clarity.

crystal **II** belonged to the $P2_1/n$ space group. Two molecules of 6,7-BDTC (the dihedral angle: 126°) were dimerized while inverting from each other by partial π–π interactions at the coumarin moiety. The π–π distances between the coumarin cores in the dimer were 3.364 and 3.367 Å. Hydrogen bonding networks consisting of C–H···O and C–H···S bonds were formed along the molecular short and long sides of 6,7-BDTC, but no significant interactions were observed in the *b*-axis, except between dimers (Fig. S32).

The emission spectra of crystals **I** and **II** closely resembled those of the powder samples (Fig. 3, λ_{em}: 504 (**I**); 511 (**II**) nm), and their quantum yields increased due to the dense immobilization of 6,7-BDTC by crystallization (Φ_F: 19 (**I**); 29 (**II**)%). However, the excitation spectrum of crystal **II** differed from those of crystal **I** and the powder samples (Fig. S26), suggesting that the origin of the luminescence process differed between crystal **II** and the other solid samples. Furthermore, the decay curve of crystal **I** was a double-exponential decay, as with that of ordinary powder, where the short-lived τ_1 is dominant (τ_1 = 1.50 ns (71%), τ_2 = 5.33 ns (29%)). Intriguingly, crystal **II** exhibited a single-exponential decay curve with only a long lifetime component (τ_1 = 6.60 ns, Table S1). The differences in lifetime components and stacking patterns between crystals **I** and **II** suggest that the origin of the fluorescent species in the solid state of 6,7-BDTC can be explained as follows. In crystal **I**, 6,7-BDTC adopts a face-to-face arrangement with strong π–π overlap, extending intermolecular interactions into 3-dimensions. Therefore, the light-blue luminescent species observed as a short-lived component is thought to originate from the delocalization of excitons in the aggregate state. The normal powder is also thought to follow this face-to-face stacking (Fig. S33). When this layered structure is disrupted by grinding, the effective intermolecular overlap collapses. As a result, the proportion of long-lived green

luminescent species, where transitions to localized excitons dominate similar to single molecules, is expected to increase within the ground powder. In contrast, in crystal **II**, 6,7-BDTC forms partially overlapping head-to-tail dimers, with intermolecular interactions extending along the *a* and *c* axes. However, no interactions are observed along the *b* axis, indicating the formation of a layer-separated stacking arrangement. Intermolecular interactions are reduced compared to crystal **I**. It is presumed that the long-lived green luminescent species was obtained as a pure component because the generated excitons prioritized localization in the layer over spatial delocalization.

In conclusion, 6,7-BDTC has been successfully synthesized and characterized. 6,7-BDTC exhibited the solvatofluorochromic effect from green to yellow in dilute solution. Also, the powder samples of 6,7-BDTC changed their emission color from light blue to green in response to mechanical stimulation. Two crystal polymorphs (crystals **I** and **II**) with different emission colors and stacking patterns were obtained. Based on the donor–acceptor structure derived from the folded skeleton, we found that suppressing the overlap of intermolecular conjugated planes through face-to-face and head-to-tail stacking formed within the molecular assembly enables the elicitation of different emission properties. Such folded dyes hold the potential to provide insights into the luminescence behavior of molecular assemblies and design guidelines for controlling the excited state.

Conflicts of interest

There are no conflicts to declare.

Data availability

The data supporting this article have been included as part of the supplementary information (SI). Supplementary information; experimental procedures, ^{1}H, ^{13}C and ^{19}F NMR charts, HRMS spectrometry data, optical properties, crystal data and crystal structures, theoretical study, video of emission color change triggered by mechanical stimulation. See DOI: https://doi.org/10.1039/d5cc05320j.

CCDC 2487912 (crystal **I**) and 2487913 (crystal **II**) contain the supplementary crystallographic data for this paper.[16a,b]

Acknowledgements

We thank Dr K. Takimoto (Kitasato University) for providing support with X-ray diffraction analysis. This research was funded by JSPS KAKENHI (grant numbers JP22K05070 and JP24K08400). The quantum calculations were performed at the Research Center for Computational Science, Okazaki, Japan (21-IMS-C188).

References

1 (*a*) T. O. Soine, *J. Pharm. Sci.*, 1964, **53**, 231; (*b*) L. Wu, X. Wang, W. Xu, F. Farzaneh and R. Xu, *Curr. Med. Chem.*, 2009, **16**, 4236; P. K. Jain and H. Joshi, *J. Appl. Pharm. Sci.*, 2012, **2**, 236; (*c*) A. M. Saleh, M. M. Y. Madany and L. González, *J. Plant Growth Regul.*, 2015, **34**, 233; (*d*) J. Sharifi-Rad, N. Cruz-Martins, P. López, E. P.-F. Lopez, N. Harun, B. Yeskaliyeva, A. Beyatli, O. Sytar, S. Shaheen, F. Sharopov, Y. Taheri, A. O. Docea, D. Calina and W. C. Cho, *Oxid. Med. Cell Longevity*, 2021, **2021**, 6492346; (*e*) D. Gupta, E. Guliani and K. Bajaj, *Top. Curr. Chem.*, 2024, **382**, 16.

2 (*a*) T. Yu, P. Zhang, Y. Zhao, H. Zhang, J. Meng and D. Fan, *Org. Electron.*, 2009, **10**, 653; (*b*) G. Signore, R. Nifosì, L. Albertazzi, B. Storti and R. Bizzarri, *J. Am. Chem. Soc.*, 2010, **132**, 1276; (*c*) R. Qian, H. Tong, C. Huang, J. Li, Y. Tang, R. Wang, K. Lou and W. Wang, *Org. Biomol. Chem.*, 2016, **14**, 5007; (*d*) W. Xue, D. Wang, C. Li, Z. Zhai, T. Wang, Y. Liang and Z. Zhang, *J. Org. Chem.*, 2020, **85**, 3689; (*e*) K. Górski, I. Deperasińska, G. V. Baryshnikov, S. Ozaki, K. Kamada, H. Ågren and D. T. Gryko, *Org. Lett.*, 2021, **23**, 6770; (*f*) Ł. Kielesiński, I. Deperasińska, O. M. Kateryna, V. Vygranenko, E. T. Ouellette and D. T. Gryko, *J. Org. Chem.*, 2022, **87**, 5961.

3 (*a*) D. Kim, Q. P. Xuan, H. Moon, Y. W. Jun and K. H. Ahn, *Asian J. Org. Chem.*, 2014, **3**, 1089; (*b*) M. Tasior, D. Kim, S. Singha, M. Krzeszewski, K. H. Ahn and D. T. Gryko, *J. Mater. Chem. C*, 2015, **3**, 1421; (*c*) Nitisha and P. Venkatakrishnan, *J. Org. Chem.*, 2019, **84**, 10679; (*d*) Nitisha and P. Venkatakrishnan, *Tetrahedron Lett.*, 2020, **61**, 15148; (*e*) A. Kumar, A. Rajpoot, F. Imroze, S. Maddala, S. Dutta and P. Venkatakrishnan, *Eur. J. Org. Chem.*, 2020, 6976; (*f*) A. Kumar and P. Venkatakrishnan, *Asian J. Org. Chem.*, 2021, **10**, 1390.

4 (*a*) A. Mukhopadhyay, T. Hossen, I. Ghosh, A. L. Koner, W. M. Nau, K. Sahu and J. N. Moorthy, *Chem. – Eur. J.*, 2017, **23**, 14797; (*b*) K. Usui, K. Yamamoto, Y. Ueno, K. Igawa, R. Hagihara, T. Masuda, A. Ojida, S. Karasawa, K. Tomooka, G. Hirai and H. Suemune, *Chem. – Eur. J.*, 2018, **24**, 14617; (*c*) A. Mukhopadhyay, K. Jana, T. Hossen, K. Sahu and J. N. Moorthy, *J. Org. Chem.*, 2019, **84**, 10658.

5 Nitisha, P. Chetti and V. Parthasarathy, *Chem. Commun.*, 2022, **58**, 431.

6 H. Liu, Y. Gao, J. Cao, T. Li, Y. Wen, Y. Ge, L. Zhang, G. Pan, T. Zhou and B. Yang, Efficient room-temperature phosphorescence based on a pure organic sulfur-containing heterocycle: folding-induced spin-orbit coupling enhancement, *Mater. Chem. Front.*, 2018, **2**, 1853.

7 Z. Zhao, X. Zheng, L. Du, Y. Xiong, W. He, X. Gao, C. Li, Y. Liu, B. Xu, J. Zhang, F. Song, Y. Yu, X. Zhao, Y. Cai, X. He, R. T. K. Kwok, J. W. Y. Lam, X. Huang, D. L. Phillips, H. Wang and B. Z. Tang, *Nat. Commun.*, 2019, **10**, 2952.

8 (*a*) R. Kotani, H. Sotome, H. Okajima, S. Yokoyama, Y. Nakaike, A. Kashiwagi, C. Mori, Y. Nakada, S. Yamaguchi, A. Osuka, A. Sakamoto, H. Miyasaka and S. Saito, *J. Mater. Chem. C*, 2017, **5**, 5248; (*b*) S. Amishiro, M. Ueda and Y. Mazaki, *Bull. Chem. Soc. Jpn.*, 2022, **95**, 1723.

9 W. Liu, J. Wang, Y. Gong, Q. Liao, Q. Dang, Z. Li and Z. Bo, *Angew. Chem., Int. Ed.*, 2020, **59**, 20161.

10 (*a*) Y. Shan, J. Sheng, Q. Zhang, M. C. A. Stuart, D.-H. Qu and B. L. Feringa, *Aggregate*, 2024, **5**, e584; (*b*) X. Niu, S. Ren, K. Wang, F. Song, X. Dong, W.-J. Guo, H.-Q. Peng, Z. Zhao, J. W. Y. Lam, Y. S. Zhao, F. Li, S.-Y. Yu and B. Z. Tang, *Aggregate*, 2025, **6**, e70003; (*c*) X. Long, Z. Ma, H. Dai, Y. Wang, H. Xie, X. Ge, Z. Yang, J. Zhao, W. Hong and Z. Chi, *Aggregate*, 2025, **6**, e70006.

11 (*a*) W. Hinrich, P. Berges, G. Klar, E. Sánchez-Martínez and W. Gunsser, *Synth. Met.*, 1987, **20**, 357; (*b*) S. Söderholm, J. Noreland, G. Olovsson, I. Olovsson, J. Helleberg and L. Engman, *Mol. Cryst. Liq. Cryst.*, 1989, **167**, 259; (*c*) J. Noreland, G. Olovsson and I. Olovsson, *Synth. Met.*, 1991, **42**, 1961.

12 (*a*) K. H. Drexhage, *Dye Laser*, ed., F. P. Schäfer, Springer-Verlag, Berlin, Heidelberg, 1973, ch. 4, p. 144; (*b*) G. Jones II, W. R. Jackson, C. Y. Choi and W. R. Bergmark, *J. Phys. Chem.*, 1985, **89**, 294.

13 J. P. Cerón-Carrasco, D. Jacquemin, C. Laurence, A. Planchat, C. Reichardt and K. Sraïdi, *J. Phys. Org. Chem.*, 2014, **27**, 4199.

14 A. E. Lanterna, M. González-Béjar, M. Frenette and J. C. Scaiano, *Photochem. Photobiol. Sci.*, 2017, **16**, 1284.

15 A. Kumar, A. Rajpoot, F. Imroze, S. Maddala, S. Dutta and P. Venkatakrishnan, *Eur. J. Org. Chem.*, 2020, 6976.

16 (*a*) CCDC 2487912: Experimental Crystal Structure Determination, 2025, DOI: 10.5517/ccdc.csd.cc2phw7b; (*b*) CCDC 2487913: Experimental Crystal Structure Determination, 2025, DOI: 10.5517/ccdc.csd.cc2phw8c.